



Density functional theory investigation on the structural, mechanical, lattice dynamical and thermal properties of nodal-line semimetals CaAgX (X: P, As)

BAHADIR SALMANKURT

Distance Education Center, Sakarya University of Applied Sciences, Sakarya 54050, Turkey

For correspondence (bsalmankurt@gmail.com)

MS received 29 September 2022; accepted 15 December 2022

Abstract. First-principles calculations based on density functional theory have been used to explore the structural, mechanical, vibrational and thermal properties of Nodal-Line Semimetal CaAgX (X = P, As) for the first time in detail. Firstly, lattice parameters are obtained, and it is found that they are in excellent agreement with previous experimental data. The calculated elastic constants for hexagonal structures satisfy mechanical stability conditions. Thus, using elastic constants, bulk modulus, B/G ratio, shear ratio, Poisson's ratio, Debye temperature and minimum thermal conductivity have been calculated. An attentive investigation of elastic and mechanical properties reveals that these compounds are brittle, and the hardest one is CaAgP, which also has the highest thermal conductivity. Also, the ionic character is dominant in the bonding mechanism for all the studied materials. These materials are also dynamically stable because negative frequencies have not been observed. Lastly, CaAgP reaches the Dulong–Petit limit ($\cong 75 \text{ J mol}^{-1} \text{ K}$) slower than CaAgAs, which agrees with previous experimental study results.

Keywords. Nodal-line semimetals; density functional theory; mechanical properties; dynamical properties; thermal properties.

1. Introduction

Very recently, topological semimetals (TS) have been of interest in materials science due to superior physical properties, such as large magnetoresistance, chiral anomaly and high carrier mobility [1–3]. Due to these properties, these materials may create a new path in developing quantum computing and spintronic devices in material science [1–13]. Thanks to the semimetal's characteristic, these materials can also be effectively used for thermoelectric materials, which can turn a thermal energy into electric energy [14]. The behaviour of electronic bands near the Fermi level makes TS differ from ordinary metals. TS can be classified into three groups; Weyl semimetal (WS), Dirac semimetal (DS) and nodal-line semimetal (NLS). For WS and DS, singly degenerate or two doubly bands cross each other at separated points in the vicinity of the Fermi level and form two-fold Weyl points or four-fold Dirac points [15]. A four-fold Dirac point with two spin-degenerated states is the characteristic feature of DS. On the other hand, the WS requires breaking of either the time-reversal symmetry or the lattice inversion symmetry in DS [16]. Both DS and WS are in the group with zero-dimensional (0D) band crossings, and their band dispersion characteristics, close to Fermi energy, are linear with all direction in k-space. However, NLS is different from others.

It has two-fold or four-fold band crossings along a one-dimensional (1D) bulk Fermi surface [17]. It is crucial to consider spin–orbit coupling for most of the topological materials. However, NLS without spin–orbit coupling can be seen. The change from NL to WS could be possible when the spin–orbital coupling is considered [18]. Also, Weng and group [18] discussed in their study that if spin–orbit coupling is ignored and band inversion occurs, it is possible to protect NLS in three-dimensional momentum space by virtue of inversion and time-reversal symmetry.

After realizing the importance of NLS, many attempts have been made to understand the characteristic of these types of materials, such as Cu_3NX (X = Ni, Cu, Pd, Ag, Cd), AX_2 (A = Ca, Sr, Ba; X = Si, Ge, Sn), CaCdSn , Mg_3Bi_3 , CaPd , TlTaSe_2 , Ca_3P_2 , CaAgX (X = As, P) and ZrXY (X = Si, Ge; Y = S, Se) [18–25]. However, most of the mentioned materials have complex band structures, which is not suitable for measuring the signals. Because it is important to get a good quantum transport signal from the nodal-line materials in the experiment [26]. So, clean, hydrogen-atom-like NLS is needed. Okamoto *et al* [27] asserted in 2016 that the simple electronic structures of CaAgP and CaAgAs make the compounds ideal for studying the physics of NLSMs due to optimal Dirac ring character at Fermi level. However, the synthesis of these

compounds was reported firstly by Mewis in 1979 [28]. Also, Wang *et al* [29] indicated that CaAgAs is the best candidate NLS predicted by theoretical study in 2017. These works motivated us to study the physical properties of CaAgX.

Thus, due to remarkable interest in the area, fundamental properties should be explored for possible future applications. Here, the first-principles study results for these compounds are reported for the first time. The materials' structural, mechanical, dynamical and thermal properties have been investigated in detail.

2. Experimental

Theoretical calculation based on density functional theory method was employed using QUANTUM ESPRESSO (QE) code [30–32]. The solution of the Kohn–Sham equation is represented by the Generalized Gradient Approximation–Perdew–Burke–Ernzerhof (GGA–PBE) method [33]. To define near-core regions, the projector-augmented wave method was used [34]. Broyden–Fletcher–Goldfarb–Shanno method was preferred to perform geometry optimization with converge criteria of 10^{-4} au [atomic unit] for the energy and 10^{-3} au for the force [35,36]. The cutoff energy for the maximum number of plane waves was taken as 50 Ry. The Bader method has been used to analyse the atoms' charge distribution [37]. To represent Brillouin zone integration on a discrete equally spaced mesh, Monkhorst–Pack mesh with a $6 \times 6 \times 10$ grid was considered [38]. Integration over the Fermi surface was employed using a Methfessel–Paxton smearing of 0.02 Ry [39]. Elastic constants have been determined using thermo_pw code [40]. Geometric structures have been portrayed using Vesta and XcrysDen software [41,42]. After performing total energy calculations, it was possible to obtain dynamical properties using the density functional perturbation theory, which provides non-supercell calculation [43]. After obtaining the dynamical matrices, the phonon frequencies have easily been produced with a Fourier interpolation for any chosen q-points. The results show that the $3 \times 3 \times 4$ grid (9 k-points in the irreducible Brillouin zone) is enough to compute dynamical matrices.

3. Result and discussion

3.1 Structural and mechanical properties

CaAgX (X = P, As) defined by the space group P-62m (D_{3h}), (No. 189) crystalline in the ZrNiAs-type structure with Wyckoff positions of 3(g) (X_{Ca} , 0, $\frac{1}{2}$) for three Ca atoms, 3(f) (X_{Ag} , 0, 0) for three Ag atoms, 2(c) ($\frac{1}{3}$, $\frac{2}{3}$, 0) for two P(1) atoms, and 1(b) (0, 0, $\frac{1}{2}$) for one P(2) atom [28,44]. Related crystal structures are shown in figure 1.

After the complete structural optimization calculations have been carried out, lattice constant parameters a , c and

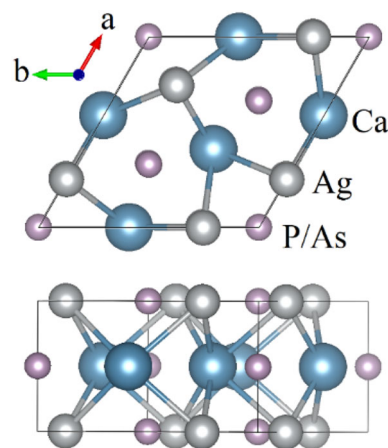


Figure 1. Crystal structure of CaAgAs and CaAgP.

c/a are obtained and presented in table 1, along with previous experimental results. It is clearly shown in the table that the obtained lattice constants values have been realized to be consistent with previous experimental data [14,24,27–29]. Thus, this agreement assures the reliability of the study. Also, the bulk modulus (B) using the Murnaghan equation of states has been conducted and given in table 1 [45].

Elastic parameters are significant because they provide information linked to mechanical properties, such as hardness and brittleness [25]. For example, the magnitude of mechanical response under shearing and uniaxial deformations are related to Shear and Young's modulus, respectively [46]. To get the elastic parameter, the individual elastic constants, C_{11} , C_{12} , C_{13} , C_{33} , C_{44} , should be considered for hexagonal structure systems [47]. Elastic parameters given in table 2 have been calculated for the first time in the area. Before examining the mechanical properties, it should be known that mechanical stability must be ensured with the criteria given in equation (1).

$$C_{11} > |C_{12}|; \quad (C_{11} + 2C_{12})C_{33} - 2C_{13}^2 > 0; \quad C_{44} > 0 \quad (1)$$

Table 1. Calculated lattice constants and Bulk modulus (B).

		a (Å)	c (Å)	c/a	B (GPa)
CaAgP	This work	7.04	4.18	0.59	68
	Exp [28]	7.045 [1]	4.174 [1]		
	Exp [27]	7.0431 [6]	4.1614 [4]		
	Exp [14]	7.0515 [1]	4.1777 [1]		
CaAgAs	This work	7.22	4.29	0.59	60
	Exp [28]	7.204 [1]	4.270 [1]		
	Exp [27]	7.2127 [9]	4.2718 [5]		
	Exp [24]	7.2041 [1]	4.2699 [1]		
	Exp [29]	7.201	4.263		

Table 2. The calculated elastic constants (in GPa).

	C_{11}	C_{12}	C_{13}	C_{33}	C_{44}	C_{66}
CaAgP	123	38	41	125	45	43
CaAgAs	108	33	37	110	39	37

According to this criterion, the calculated elastic parameters have provided the mechanical stability of the materials in the hexagonal structure [47]. So, the mechanical properties can be conveniently examined.

Bulk modulus defines a material's reaction to volumetric stress [48]. Generally, a softer material can be related to a low bulk modulus, but the importance of the Shear modulus cannot be ignored and should be considered. In case of a mismatch between B and G, it would be plausible to take notice of the Shear modulus while concluding the softness [49]. As can be seen from table 3, the lowest bulk and Shear modulus belong to CaAgAs, which is the softest material practiced in this study.

Besides this, the studied crystals are harder to be compressed along the c-direction compared to a-direction since the value of C_{11} has a larger value than that of C_{33} for all compounds. Also, the value of C_{12} for CaAgX is lower than that of C_{13} , which indicates that if the stress along the a-direction is applied, the strain occurring in the c-direction will be larger compared to the b-direction a fat lot.

The value of B/G (Pugh) ratio can be utilized to bring into the open the brittleness or ductility characteristic of these crystals, and the critical value is 1.75. If the B/G ratio of any material is higher than 1.75, then it has a ductile manner [50]. The data in table 3 shows that CaAgP and CaAgAs are brittle.

The stiffness of the material can be realized by Young's modulus E . The crystal becomes softer if the value of E is low [51]. According to table 3, CaAgAs is softer by 15% than CaAgP.

Poisson's ratio is a good indicator to determine the ionic or covalent bonding nature of the materials [52]. The crystal has dominantly covalent bonding if Poisson's ratio is about 0.1, while the value of 0.25 represents the ionic bonding. The bonding character of the materials can be easily seen in

Table 3. Bulk modulus (in GPa) is given along with the calculated Shear modulus (G in GPa), Poisson's ratio (ν) and Pugh ratio (B/G).

	B	G	E	ν	B/G
CaAgP	68(68)	43	107	0.24	1.57
CaAgAs	60(61)	38	93	0.24	1.60

The Bulk modulus obtained by Murnaghan's equation of states are displayed in brackets.

table 3, where the values are 0.24, implying that the materials have an ionic bonding nature. This is also consistent with Bader charge analysis results given in table 4.

After that, Θ_D (Debye temperature) is calculated, and its formula is given in equation (2). There is a robust correlate between the melting point and Θ_D , where Θ_D is around 30–50% of the melting temperature [53]. Moreover, Θ_D can be regarded as a measure of the softness of the crystal and is prominent for determining thermal conductivity [54]. So, it is essential to calculate the Θ_D .

$$\Theta_D = \frac{h}{k_B} V_M \left(\frac{3n N_A \rho}{4\pi M} \right)^{1/3} \quad (2)$$

where ρ , n , M , k_B , h and N_A are mass density, the number of atoms in the molecule, molecular weight, Boltzmann constant, Planck's constant and Avogadro's number, respectively. Furthermore, the elastic wave velocity, which can also be described as sound velocity, is given in equation (5).

$$v_l = \sqrt{\frac{3B + 4G}{3\rho}} \quad (3)$$

$$v_t = \sqrt{\frac{G}{\rho}} \quad (4)$$

$$v_m = \left[\frac{1}{3} \left(\frac{2}{v_l^3} + \frac{1}{v_t^3} \right) \right]^{-1/3} \quad (5)$$

where v_l , v_t and v_m are longitudinal, transverse and average sound elastic wave velocities, respectively.

It can be deduced from table 5 that the value of Θ_D of CaAgP is higher compared to CaAgAs mainly due to the speed of acoustic (elastic) waves. This value also implies the soft character of CaAgAs.

The minimum thermal conductivity can be attained by using Cahill's model [55] with the formula given in equation (6).

$$k_{\min} = \frac{k_B}{2.48} n^{\frac{2}{3}} (v_l + 2v_t) \quad (6)$$

As seen from table 5, the order of k_{\min} from high to low is produced to be in the given order; CaAgP > CaAgAs. This order points out that thermal conductivity is the best for CaAgP.

Table 4. The Bader partial net charges for CaAgX (units are in |e|).

	Ca	Ag	X
CaAgP	+1.36	- 0.11	- 1.25
CaAgAs	+1.35	- 0.18	- 1.17

Positive indicates missing electrons, while negative means additional electrons.

Table 5. The calculated density (ρ), transverse, longitudinal and average elastic (sound) velocities (V_t , V_l and V_m), Debye temperature (Θ_D) and minimum thermal conductivity k_{\min} .

Compounds		ρ (g cm ⁻³)	V_t (m s ⁻¹)	V_l (m s ⁻¹)	V_A (m s ⁻¹)	Θ_D (K)	k_{\min} (Wm ⁻¹ K ⁻¹)
CaAgP	Present	4.97	2950	5026	3270	359	0.83
	Exp [28]	4.91					
	Theo [28]	4.97					
CaAgAs	Present	5.78	2559	4381	2838	304	0.68
	Exp [28]	5.76					
	Theo [28]	5.78					

3.2 Vibrational properties

Because of the fact that primitive unit cells of the materials have been composed of three crystal formulas (nine atoms in total), there should be 3 acoustic and 24 optical phonon modes, which can be viewed in figure 2. This figure also indicates that these materials are stable in hexagonal structure at ground state, because there are no negative phonon branches along all symmetry directions.

For these semimetals, overlapping the acoustic branches and optical branches of phonon curves can be seen and are not separated by a gap. However, a small bandgap is observed at 111 cm⁻¹ of CaAgP, located between optical branches.

As stated previously, the space group of mentioned compounds in this work is P-62m, whose point group (D_{3h}) have six different types of irreducible representations

E' , E'' , A'_1 , A''_1 , A'_2 and A''_2 [56]. At the outset, Gamma [zone-centre] point optical phonon modes have been considered as they have a crucial role in defining Raman and infrared (IR) spectra in the materials [57]. Nonetheless, Brillouin zone-centre optical phonon modes of the compounds can be expressed as in equation (7).

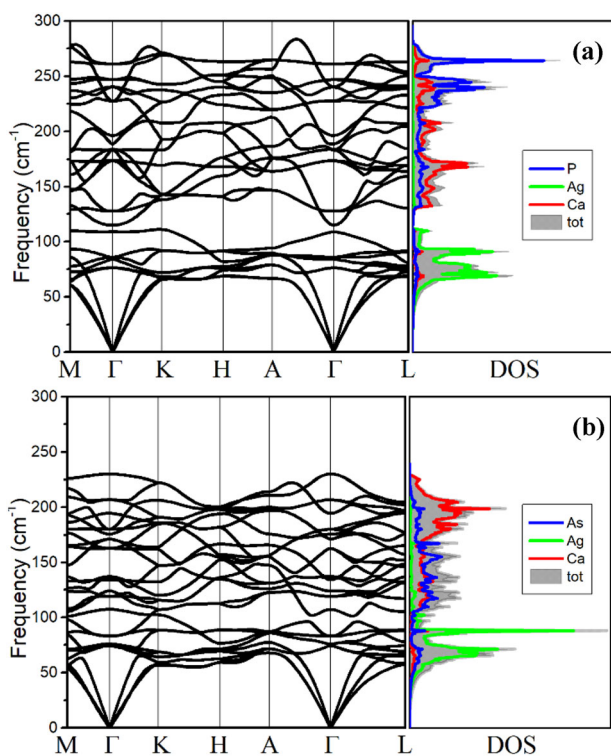
$$\Gamma_{\text{optic}} = 6E' + 2E'' + 2A'_1 + A''_1 + 2A'_2 + 3A''_2, \quad (7)$$

where double and single degenerate modes belong to E and A modes, respectively. These modes are given in table 6.

As can be seen from figures 3 and 4, the vibration of the E'' , A''_1 and A''_2 modes in the materials occur along the c-direction. Among them, A''_1 mode is silence, which indicates that it cannot be identified by either Raman or IR. This mode is unique because it represents only the opposite vibration of P (or As) atoms occupied at Wyckoff position of 2(c) (1/3, 2/3, 0). A''_1 mode of CaAgP is much higher (59%) than CaAgAs. This is the most significant difference in the modes of the same type, the value of A''_1 changes from 197 to 124 cm⁻¹ when replacing P with As atom. Withal, only IR active mode is A''_2 involved all atoms in the vibration.

Table 6. The calculated Brillouin zone-centre phonon modes and related energies (in cm⁻¹).

Active	Modes	CaAgP	CaAgAs
I+R	E'	86	74
I+R	E'	127	119
I+R	E'	184	137
I+R	E'	228	171
I+R	E'	261	180
I+R	E'	247	207
R	E''	76	76
R	E''	174	163
R	A'_1	109	107
R	A'_1	189	176
Silence	A''_1	197	124
Silence	A'_2	84	83
Silence	A'_2	240	230
I	A''_2	240	195
I	A''_2	115	83
I	A''_2	183	134

**Figure 2.** The obtained phonon dispersion curves and phonon density of states of CaAgX.

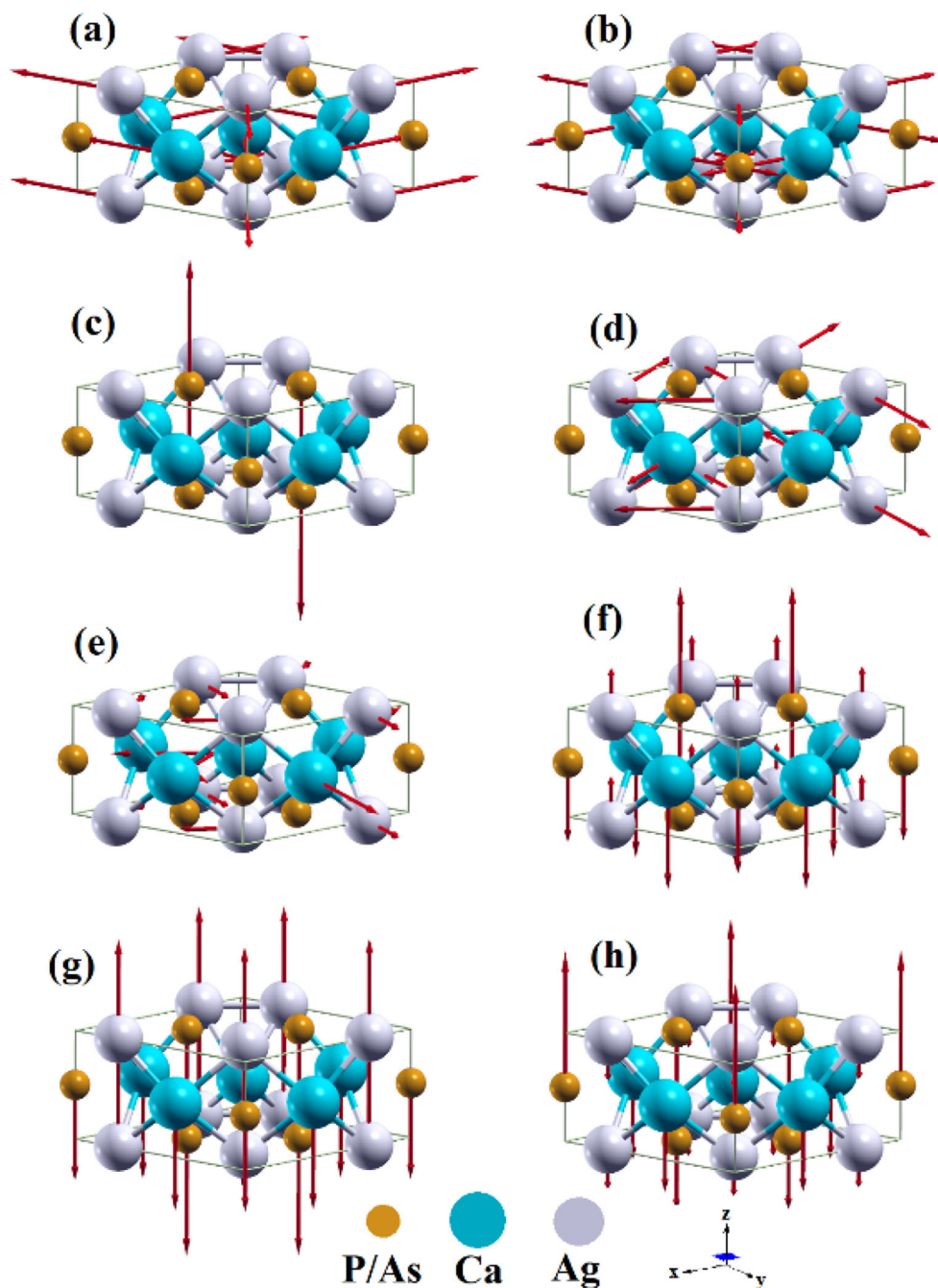


Figure 3. Eigen vectors of A_1', A_1'', A_2' and A_2'' modes for CaAgX at Gamma point. (a) A_1' (109 cm^{-1}), (b) A_1' (189 cm^{-1}), (c) A_1'' (197 cm^{-1}), (d) A_2' (84 cm^{-1}), (e) A_2' (240 cm^{-1}), (f) A_2'' (240 cm^{-1}), (g) A_2'' (115 cm^{-1}) and (h) A_2'' (183 cm^{-1}). The values given in the bracket belong to CaAgP compound.

However, E'' , two doubly degenerate modes, is raised from the vibration of Ca and Ag atoms and is Raman active. Another two doubly degenerate is Raman + IR active mode E' governed by the motion of Ca and Ag atoms on the ab-plane. Furthermore, two silence modes are represented with non-degenerate A_2' , consisting of the motion of Ca and Ag atoms on ab-plane. Lastly, A_1' is Raman active and there is a lack of vibration of P (or As) in any direction for this mode.

In general, the energies of optical phonon bands of the crystal increase with decreasing atomic weight. Thus, the energy of those bands decreases when replacing P with As atom. This is mainly due to the strength of interatomic bonds affected by the differences in mass.

Next, the phonon density of states is examined to understand deeply the vibrational properties of the material from a different perspective. The right panel of figure 2 shows phonon density of states for all compounds.

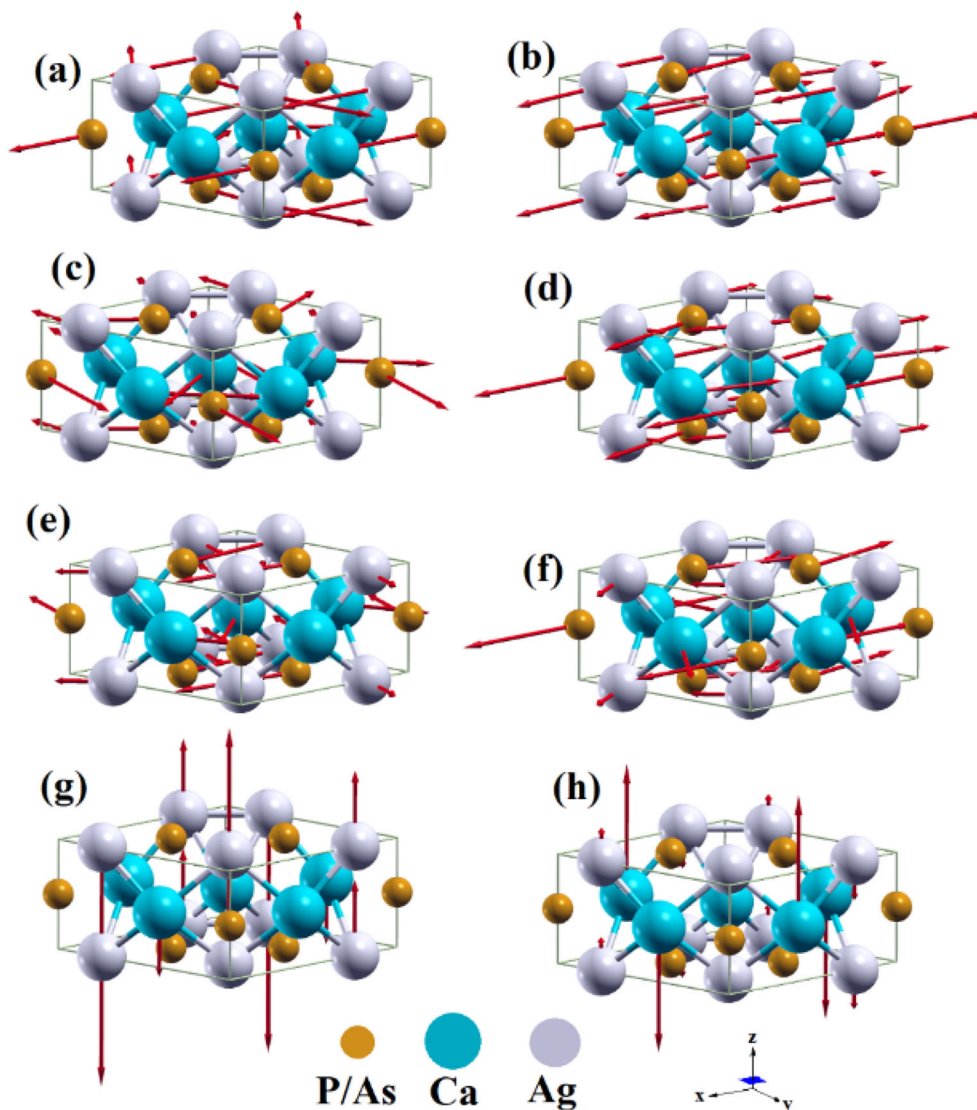


Figure 4. Eigen vectors of E' and E'' modes for CaAgX at Gamma point. (a) E' (86 cm^{-1}), (b) E' (127 cm^{-1}), (c) E' (184 cm^{-1}), (d) E' (228 cm^{-1}), (e) E' (261 cm^{-1}), (f) E' (247 cm^{-1}), (g) E'' (76 cm^{-1}) and (h) E'' (174 cm^{-1}). The values given in the bracket belong to CaAgP compound.

The sharpest peak of CaAgAs, quite a lot contributed by Ag atoms, is about 75 cm^{-1} and comes from the flatness of phonon dispersion along all directions. Contribution to this peak from Gamma point belongs to E'' mode at 75 cm^{-1} , where most of the vibration corresponds to Ag atom motion. However, the peak at 200 cm^{-1} comes from the optical phonon branch, which is nearly flat along the K–H–A symmetry directions.

On the other hand, the most striking feature of the CaAgP phonon density of states is the sharp peak at 264 cm^{-1} , where the P atom contribution is dominant since its atomic mass is much smaller than the other atoms. This peak is formed by the flatness of the phonon branch along all directions, and its gamma point mode is E' .

As seen from figure 2, the Ag atom contribution to the low energy phonon modes (Acoustic modes) region is

dominant for both CaAgP and CaAgAs. However, the contribution to the highest energy optical phonon frequency regions for CaAgP ($225 - 275 \text{ cm}^{-1}$) and CaAgAs ($175 - 225 \text{ cm}^{-1}$) is provided by P and Ca atoms, respectively.

3.3 Thermal properties

In this section, the Helmholtz-free energy, the internal energy, the constant volume specific heat, and the entropy as functions of temperature are executed. Thermodynamic functions mentioned above can be determined using the vibrational degrees of freedom of the lattice, because, in general, the electronic degrees of freedom play an insignificant role in the materials except for only metals at very low temperatures [58].

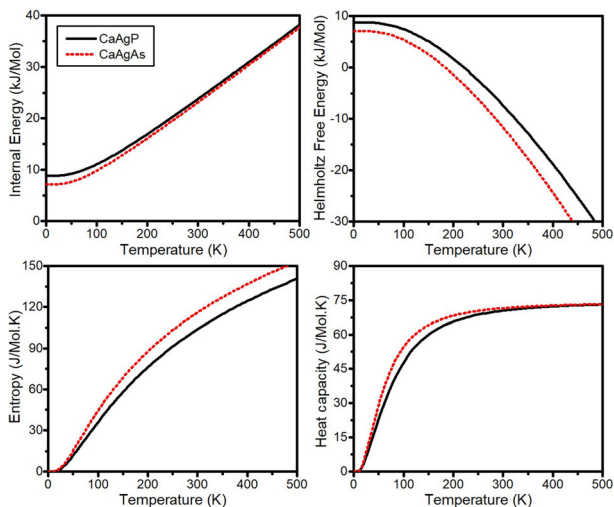


Figure 5. Temperature dependence of thermal properties of CaAgX.

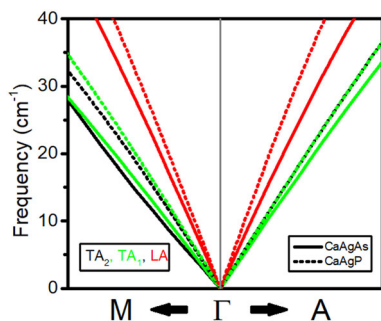


Figure 6. The theoretical results of TA (indicated as black and green colour) and LA (indicated as red colour) phonon branches in the selected region of the wave vector ($2\pi/a$). Solid lines indicate CaAgAs and dashed lines correspond to CaAgP.

However, a solid knowledge of the phonon dispersion curves, with adequate accuracy, is needed for the calculation of these thermodynamic functions using quasi-harmonic approximation [59],

$$E = \frac{3nN\hbar}{2} \int_0^\infty w \coth\left(\frac{\hbar w}{2k_B T}\right) F[w] dw \quad (8)$$

$$F = 3nNk_B T \int_0^\infty \ln \left[2 \sinh\left(\frac{\hbar w}{2k_B T}\right) \right] F[w] dw \quad (9)$$

$$S = 3nNk_B \int_0^\infty \left(\frac{\hbar w}{2k_B T} \coth\left(\frac{\hbar w}{2k_B T}\right) - \ln \left[2 \sinh\left(\frac{\hbar w}{2k_B T}\right) \right] \right) F[w] dw \quad (10)$$

The phonon-specific heat C_V measures how well the crystal can hold energy with rising temperatures [60]. Figure 5 shows the characteristic behaviour of C_V , where the temperature dependence slowly diminishes at high temperatures, and the C_V value is almost fixed at Dulong–Petit limit ($\cong 75 \text{ J mol}^{-1} \text{ K}$), as expected. Here, CaAgAs reaches to the Dulong–Petit limit faster than CaAgP, consistent with previous experimental study results [27].

The thermal stability of a material is connected with Helmholtz-free energy [50]. Helmholtz-free energy of CaAgAs has a lower value than that of CaAgP, meaning that the worst thermal stability belongs to CaAgAs.

The contribution of low phonon frequencies can be understandable with the behaviour of entropy. The higher the entropy value, the more the contribution from low phonon frequencies [50]. In figure 5, it is unambiguously demonstrated that the contribution from low phonon frequencies should be highest for CaAgAs, which can be, therefore, verified by the phonon band structure, given in figure 2.

The maximum oscillation frequency is important to determine thermal conductivity. This frequency is called Debye frequency, highly associated with Θ_D . In light of this information, a higher maximum oscillation frequency belongs to CaAgP. So, Θ_D of CaAgP should be higher than that of CaAgAs. As we can see from table 5, this is consistent with results obtained by elastic constants.

The thermal conductivity is also related to acoustic velocity. Acoustic velocity can be understandable with small k-wave vector phonon mode slope and elastic constants [61]. First, the phonon mode slope is examined. The absolute value of the phonon mode slope in a given direction is directly proportionate to acoustic velocity. A slope with a greater absolute value indicates a faster acoustic velocity. So, the larger slope means a higher thermal conductivity. It can be seen from figure 6 that the slopes of TA (transverse acoustic) and LA (longitudinal acoustic) modes of CaAgP are larger than those of CaAgAs. This indicates that the highest thermal conductivity belongs to CaAgP crystal.

Second, the relation between elastic constants and acoustic velocities is investigated, and relevant formulas are given by the following;

Table 7. The calculated TA and LA velocities (in m s^{-1}).

	CaAgP $\Gamma - A$ ([001])	CaAgP $\Gamma - M$ ([100])	CaAgAs $\Gamma - A$ ([001])	CaAgAs $\Gamma - M$ ([100])
V_{LA}	5015	4975	4362	4323
V_{TA1}	3009	2941	2598	2530
V_{TA2}	3009	3009	2598	2598

(1) along the $\Gamma - A([001])$ direction;

$$\begin{aligned} [001]V_{LA} &= \sqrt{C_{33}/\rho} \\ [100]V_{TA} &= \sqrt{C_{44}/\rho} \end{aligned} \quad (11)$$

(2) along the $\Gamma - M([100])$ direction;

$$\begin{aligned} [100]V_{LA} &= \sqrt{C_{11}/\rho} \\ [010]V_{TA1} &= \sqrt{C_{66}/\rho} \\ [001]V_{TA2} &= \sqrt{C_{44}/\rho} \end{aligned} \quad (12)$$

The results in table 7 show that CaAgAs has lower thermal conductivity than CaAgP.

Here, the thermal conductivity has been investigated in different ways and compared among the mentioned materials.

4. Conclusion

In this study, the fundamental physical properties of NLS CaAgX have been reported using density functional theory for the first time in detail. The calculations have been executed within the GGA-PBE method. There is an excellent agreement between the obtained lattice parameters and previous experimental data. The change of X atoms leads to an insignificant change in the lattice parameters of all the mentioned materials, which, as a matter of course, affect the mechanical, thermal and vibrational properties. The Bulk modulus values obtained by Murnaghan's equation of state are very close to the values calculated from the Thermo-PW code. The calculated elastic parameters satisfy mechanical stability. Brittle character is dominant for CaAgP and CaAgAs. Besides this, Bader Charge Analysis results demonstrate that the materials have dominantly ionic bonding, supported by Poisson's ratio results. Next, the order of Debye temperature is $\text{CaAgP} > \text{CaAgAs}$, indicating that CaAgP has the highest thermal conductivity and the strongest chemical bonds. Afterwards, vibrational and thermal properties are obtained. One can easily deduce from the phonon figures that NLS compounds are dynamically stable in a hexagonal structure. A phonon bandgap is available only for CaAgP. The highest energy optical mode at the Gamma point is directly associated with A'_2 (230 cm^{-1}) and E' (261 cm^{-1}) modes for CaAgAs and CaAgP, respectively. Furthermore, the thermal properties have been employed using quasi-harmonic approximation. This work will be helpful for future studies.

References

- [1] Zhang X, Jin L, Dai X and Liu G 2017 *J. Phys. Chem. Lett.* **8** 4814
- [2] Hosen M M, Dimitri K, Belopolski I, Maldonado P, Sankar R, Dhakal N *et al* 2017 *Phys. Rev. B* **95** 161101
- [3] Xu Q, Yu R, Fang Z, Dai X and Weng H 2017 *Phys. Rev. B* **95** 045136
- [4] Gao H, Venderbos J W, Kim Y and Rappe A M 2019 *Annu. Rev. Mater. Res.* **49** 153
- [5] Li Z H, Wang W, Zhou P, Ma Z S and Sun L Z 2019 *New J. Phys.* **21** 033018
- [6] Takane D, Nakayama K, Souma S, Wada T, Okamoto Y, Takenaka K *et al* 2018 *NPJ Quantum Mater.* **3** 1
- [7] Kwan Y H, Reiss P, Han Y, Bristow M, Prabhakaran D, Graf D *et al* 2020 *Phys. Rev. Res.* **2** 012055
- [8] Chen C, Wang S S, Liu L, Yu Z M, Sheng X L, Chen Z *et al* 2017 *Phys. Rev. Mater.* **1** 044201
- [9] Laha A, Mardanya S, Singh B, Lin H, Bansil A, Agarwal A *et al* 2020 *Phys. Rev. B* **102** 035164
- [10] Xu N, Qian Y T, Wu Q S, Autès G, Matt C E, Lv B Q *et al* 2018 *Phys. Rev. B* **97** 161111
- [11] Nayak J, Kumar N, Wu S C, Shekhar C, Fink J, Rienks E D *et al* 2018 *J. Phys. Condens. Matter* **30** 045501
- [12] Hatano T, Nakamura I, Ohta S, Tomizawa Y, Urata T, Iida K *et al* 2020 *J. Phys. Condens. Matter* **32** 435703
- [13] Okamoto Y, Saigusa K, Wada T, Yamakawa Y, Yamakage A, Sasagawa T *et al* 2020 *Phys. Rev. B* **102** 115101
- [14] Quinn R J and Bos J W G 2022 *Appl. Phys. Lett.* **120** 073903
- [15] Armitage N P, Mele E J and Vishwanath A 2018 *Rev. Mod. Phys.* **90** 015001
- [16] Burkov A A and Balents L 2011 *Phys. Rev. Lett.* **107** 127205
- [17] Yamakage A, Yamakawa Y, Tanaka Y and Okamoto Y 2016 *J. Phys. Soc. Jpn.* **85** 013708
- [18] Yu R, Weng H, Fang Z, Dai X and Hu X 2015 *Phys. Rev. Lett.* **115** 036807
- [19] Huang H, Liu J, Vanderbilt D and Duan W 2016 *Phys. Rev. B* **93** 201114
- [20] Chang T R, Pletikoscic I, Kong T, Bian G, Huang A, Denlinger J *et al* 2019 *Adv. Sci.* **6** 1800897
- [21] Liu G, Jin L, Dai X, Chen G and Zhang X 2018 *Phys. Rev. B* **98** 075157
- [22] Bian G, Chang T R, Zheng H, Velury S, Xu Y, Neupert T *et al* 2016 *Phys. Rev. B* **93** 121113
- [23] Xie L S, Schoop L M, Seibel E M, Gibson Q D, Xie W and Cava R J 2015 *APL Mater.* **3** 083602
- [24] Emmanouilidou E, Shen B, Deng X, Chang T R, Shi A, Kotliar G *et al* 2017 *Phys. Rev. B* **95** 245113
- [25] Salmankurt B and Duman S 2017 *Philos. Mag.* **97** 175
- [26] Zhou T, Tong M, Xie X, Yu Y, Zhu X, Wang Z Y *et al* 2020 *J. Phys. Chem. Lett.* **11** 6475
- [27] Okamoto Y, Inohara T, Yamakage A, Yamakawa Y and Takenaka K 2016 *J. Phys. Soc. Jpn.* **85** 123701
- [28] Mewis A 1979 *Z. Naturforsch. B* **34** 14
- [29] Wang X B, Ma X M, Emmanouilidou E, Shen B, Hsu C H, Zhou C S *et al* 2017 *Phys. Rev. B* **96** 161112
- [30] Hohenberg P and Kohn W 1964 *Phys. Rev.* **136** 864
- [31] Kohn W and Sham L 1965 *Phys. Rev.* **140** 1133
- [32] Giannozzi P, Baroni S, Bonini N, Calandra M, Car R, Cavazzoni C *et al* *J. Phys. Condens. Matter* **21** 395502
- [33] Seidl A, Görling A, Vogl P, Majewski J A and Levy M 1996 *Phys. Rev. B* **53** 3764
- [34] Blöchl P E 1994 *Phys. Rev. B* **50** 17953
- [35] Fischer T H and Almlof J 1992 *J. Phys. Chem.* **96** 9768
- [36] Pfrommer B G, Cote M, Louie S G and Cohen M L 1997 *J. Comput. Phys.* **131** 233

- [37] Tang W, Sanville E and Henkelman G 2009 *J. Phys. Condens. Matter* **21** 084204
- [38] Monkhorst H J and Pack J D 1976 *Phys. Rev. B* **13** 5188
- [39] Methfessel M P A T and Paxton A T 1989 *Phys. Rev. B* **40** 3616
- [40] Giannozzi P, Andreussi O, Brumme T, Bunau O, Nardelli M B, Calandra M *et al* 2017 *J. Phys. Condens. Matter* **29** 465901
- [41] Kokalj A 1999 *J. Mol. Graph.* **17** 176
- [42] Momma K and Izumi F 2008 *J. Appl. Crystallogr.* **41** 653
- [43] Baroni S, Gironcoli S, Dal Corso A and Giannozzi P 2001 *Rev. Mod. Phys.* **73** 515
- [44] Hirose H T, Terashima T, Wada T, Matsushita Y, Okamoto Y, Takenaka K *et al* 2020 *Phys. Rev. B* **101** 245104
- [45] Murnaghan F D 1944 *Proc. Natl. Acad. Sci.* **30** 244
- [46] Hu C W, Yang Y, Hou C and Liang T X 2020 *Mater. Today Commun.* **25** 101619
- [47] Zhang X, Wang F, Li Z and Jiang W 2016 *Mater. Lett.* **185** 389
- [48] Yalcin B G, Salmankurt B and Duman S 2016 *Mater. Res. Express* **3** 036301
- [49] Bağcı S, Cin M, Uzunok H Y, Karaca E, Tütüncü H M and Srivastava G P 2019 *Phys. Rev. B* **100** 184507
- [50] Salmankurt B and Duman S 2016 *Mater. Res. Express* **3** 045903
- [51] Liu H, Liu Z T, Ren J and Liu Q J 2017 *Solid State Commun.* **251** 43
- [52] Ciftci Y O, Ozayman M, Surucu G, Colakoglu K and Deligoz E 2012 *Solid State Sci.* **14** 401
- [53] Duc N B, Hieu H K, Hanh P T M, Hai T T, Tuyen N V and Ha T T 2020 *Eur. Phys. J. B* **93** 1
- [54] Anderson O L 1963 *J. Phys. Chem. Solids* **24** 909
- [55] Cahill D G, Watson S K and Pohl R O 1992 *Phys. Rev. B* **46** 6131
- [56] Powell R C 2010 *Symmetry, group theory, and the physical properties of crystals* (New York: Springer-Verlag)
- [57] Charifi Z, Baaziz H, Noui S, Uğur Ş, Uğur G, Iyigör A *et al* 2014 *Comput. Mater. Sci.* **87** 187
- [58] Soyalp F, Yavuz M and Yalçın Z 2013 *Comput. Mater. Sci.* **77** 72
- [59] Palumbo M and Dal Corso A 2017 *J. Phys. Condens. Matter* **29** 395401
- [60] Böer K W and Pohl U W 2018 *Semiconductor physics*. Springer Cham, New York
- [61] Cong X, Li Q Q, Zhang X, Lin M L, Wu J B, Liu X L *et al* 2019 *Carbon* **149** 19